Evaluation of Seismic Design Parameters for Modular Metal Buildings in High Seismic Zones

MOHAMMAD T. NIKOUKALAM, SHAHABEDDIN TORABIAN, and BENJAMIN W. SCHAFER

ABSTRACT

The objective of this paper is to evaluate the seismic design parameters for modular metal building systems in high seismic zones in the United States using the FEMA P695 (ATC, 2009) methodology. Modular metal buildings, commonly used for large open spaces such as warehouses and data centers, combine traditional built-up tapered steel frames with intermediate gravity-only columns. A suite of archetype buildings with varying spans, heights, and number of modules was developed in collaboration with industry and analyzed using nonlinear static and dynamic procedures. High-fidelity shell finite element models, validated against component and shake table tests, capture key failure modes, including local and global buckling. Results from pushover and quasi-static cyclic analyses were used to calibrate nonlinear single-degree-of-freedom models for subsequent incremental dynamic analyses against the FEMA P695 earthquake suite. The study demonstrates that modular metal buildings designed with a response modification factor $R = 3.5$ meet the FEMA P695 collapse performance criteria, provided that lateral bracing systems are designed to meet both strength and stiffness requirements of AISC 360. Buildings using traditional strength-only bracing exhibited limited ductility due to premature column buckling, whereas AISC-compliant bracing achieved stable post-peak response and improved collapse margins. A collapse drift limit of 6% is proposed based on system flexibility and observed behavior. The findings confirm the adequacy and applicability of current ASCE 7 ordinary moment frame provisions for modular metal building systems, with important implications for design practice in high-seismic regions.

Keywords: metal buildings, seismic performance, nonlinear, incremental dynamic analysis, fragility.

INTRODUCTION

Metal building systems in the United States typically consist of I-shaped structural steel frames built up from plate and tapered (particularly in depth) to meet dominant demands, secondary cold-formed steel purlins and girts connecting from frame to frame, diagonal rod bracing to provide diaphragm and cross-frame stiffness, and finished with walls of either steel sheeting or tilt-up concrete panels with roofs of through-fastened or standing seam metal panels. For long-span metal buildings, it is common to support the main frame periodically with gravity columns—creating a "modular" metal building system—as opposed to shorter span systems without interior gravity columns known as "clear-span" metal buildings. It is common to utilize noncompact and slender sections within the tapered main frames to provide sufficient stiffness and necessary strength. For seismic design (in the frame direction), metal building systems are typically categorized as ordinary moment frames (OMFs) and thus are only required to meet the design provisions of AISC 360, *Specification for Structural Steel Buildings* (2016), hereafter referred to as AISC 360. Metal building systems have commonly performed well in earthquakes, but there has been keen interest over the last 20 years to better understand the seismic design of these systems (Uang et al., 2011; Smith, 2013; Hatch, 2014).

In particular, the experimental work led by Uang at the University of California–San Diego (UCSD) has provided important benchmarks for predicting the performance of metal building systems and components. Quasi-static cyclic tests on a 20 ft × 60 ft (6.1 m × 18.3 m) clear-span primary frame demonstrated elastic behavior up to approximately 2.5% drift, beyond which stiffness and strength degraded due to lateral-torsional buckling (LTB) in the column (Hong and Uang, 2006). Cyclic component testing of column-knee-rafter connections demonstrated that large drifts were accompanied by LTB in the rafter between brace points, along with flange local buckling (FLB), and the members could undergo multiple cycles and large drifts (beyond 6%) without fracture, but with strength loss. Comparisons of test results with AISC Design Guide 25, *Frame Design Using Web-Tapered Members* (Kaehler et al., 2011), demonstrated that accurate prediction of LTB capacity requires explicit consideration of bracing conditions.

Mohammad T. Nikoukalam, PhD, PE, Consulting Engineer, Simpson Gumpertz & Heger Inc., Washington D.C. Email: mtnikoukalam@sgh.com

Shahabeddin Torabian, PhD, PE, SE, Senior Project Manager, Simpson Gumpertz & Heger Inc., Washington D.C. Associate Scientist, Department of Civil and Systems Engineering, Johns Hopkins University, Baltimore, Md. Email: storabian@sgh.com (corresponding)

Benjamin W. Schafer, PhD, PE, Consulting Principal, Simpson Gumpertz & Heger Inc., Washington D.C., Willard and Lillian Hackerman Professor, Department of Civil and Systems Engineering, Johns Hopkins University, Baltimore, Md. Email: schafer@jhu.edu

Paper No. 2025–07

Finally, full-scale shake table testing of three clear-span metal buildings to evaluate seismic performance under varying configurations, including light and heavy wall cladding and mezzanines, was performed at UCSD (Figure 1) (Uang et al., 2011; Smith, 2013). The tests demonstrated significant system overstrength, with all specimens remaining stable up to 150% of the Imperial Valley ground motion scaled to ASCE 7-16, *Minimum Design Loads and Associated Criteria for Buildings and Other Structures* (2016), design earthquake (DE) levels, and one specimen tested up to 300% DE without collapse. [Note: Maximum considered earthquake levels, (MCE) are 150% DE.] Maximum drift ratios experienced across the specimens varied from 3.5% to 5.4% and LTB, FLB, and panel zone buckling and yielding were observed in the specimens. The buildings with heavy wall attachments exhibited limit states at earlier drifts than those with light walls. None of the buildings collapsed under the imposed excitations, and the tests stopped due to other experimental limitations on the shake table.

To complement the experimental findings, high-fidelity finite element modeling has become essential for evaluating seismic performance, particularly in utilizing the FEMA P695, *Quantification of Building Seismic Performance Factors* (ATC, 2009), procedure to validate seismic response modification coefficients (e.g., R). The second and third authors of this paper were part of a team that developed a peer-reviewed seismic modeling procedure for the seismic performance of clear-span metal buildings shaking in the direction of the main frames (Meimand et al., 2018; Moen et al., 2019). The overall approach utilized a high-fidelity, primarily shell, finite element model of the metal building system to characterize the nonlinear static hysteretic response of the frame and a nonlinear single degree of freedom model to perform the required incremental dynamic analyses (IDA) across a suite of earthquakes to assess the predicted collapse margin ratio. The high-fidelity model incorporated all typical metal building details, including flange braces, metal roof panels, and rod bracing, and was validated against component testing of the main frame and the shake table tests at UCSD (Moen et al., 2019). The peer-reviewed P695 study confirmed the applicability of the OMF seismic response modification coefficient $R = 3.5$ for both traditional light walls and tilt-up heavy walls for clear-span metal buildings (Meimand et al., 2018; Moen et al., 2019). Highlights of the overall findings from this work included (1) clear-span metal building systems are unique in that the gravity and lateral framing systems are combined and member depths and details are influenced prominently by both gravity and lateral demands in the same frame; (2) the period of metal buildings is typically longer than empirical expressions provided in ASCE 7 (ASCE, 2016), and therefore, story drifts (even within the elastic regime) are often greater than conventional steel-frame building systems; and (3) the bracing connected between the purlins or girts and the main frame is critical to achieving a stable large lateral deformation response even as global (e.g., lateral-torsional) buckling initiates.

Beyond the United States, similar modeling efforts have been undertaken to investigate the seismic performance of both clear-span and modular metal building systems in Canada (Bagatini Cachuço, 2021; Bagatini Cachuço and Yang, 2021) and provide guidance on appropriate seismic

Fig. 1. Assembled specimen on shaking table (Smith et al., 2013).

Table 1. Metal Building Archetypes Dimensions and Design Loads				
Archetype	H ft (m)	N × Span N × ft (m)	Bay ft (m)	V_r kips (kN)
AM1	25 (7.6)	2 × 50 (15.2)	25 (7.6)	17.6 (78.3)
AM2	25 (7.6)	3 × 50 (15.2)	25 (7.6)	25.6 (113.9)
AM3	45 (13.7)	2 × 50 (15.2)	25 (7.6)	18.6 (82.7)
AM4	45 (13.7)	3 × 50 (15.2)	25 (7.6)	26.6 (118.3)
AM5	25 (7.6)	2 × 100 (30.4)	25 (7.6)	33.8 (150.2)
AM6	45 (13.7)	2 × 100 (30.4)	25 (7.6)	34.8 (154.8)

response modification coefficients for use in equivalent lateral force procedures in the National Building Code of Canada (NBCC). The analytical framework employed included shell finite element models of components (e.g., the column-knee-rafter segment) in ABAQUS (Simulia, 2014) then utilized to calibrate a beam finite element model of the main frame implemented in OpenSees (McKenna et al., 2004). IDA was conducted on the OpenSees model for a suite of earthquake motions relevant to western Canada. The researchers performed a series of trial designs considering different levels of assumed ductility-based seismic force reductions (in Canada overstrength and ductility seismic force reductions are separated into two parts) and concluded that the ductility-based force reductions should be approximately 1.3 for metal buildings in western Canada.

The research reported herein uses the framework of Moen et al. (2019) to evaluate the seismic response modification coefficients for modular metal building systems in high-seismic regions in the United States. A series of modular metal building system archetypes are designed in collaboration with industry. A high-fidelity shell finite element model of the archetypes is developed and exercised through modal analysis, geometric and material nonlinear static pushover analysis, and geometric and material nonlinear static cyclic analysis. A nonlinear single degree of freedom surrogate model is calibrated to the high-fidelity model and utilized for IDA across the FEMA P695 earthquake suite. Formal P695 evaluation is performed to assess the adequacy of the assumed seismic response modification coefficients. The scope is limited to modular metal buildings up to 45 ft (13.7 m) in eave height and with roof loads no greater than 20 psf (0.96 kN/m^2) in high-seismic zones.

DESIGN OF MODULAR METAL BUILDING ARCHETYPES

A critical step in the assessment of seismic performance modification factors per FEMA P695 is the development of system archetypes. Previously, for clear-span metal buildings, four archetypes covering light and heavy walls and ranges of height-to-span for the main frames consistent with known practice were developed (Moen et al., 2019). For modular metal buildings, six archetypes were developed, as summarized in Table 1 and depicted in Figure 2. The buildings cover heights of 25 ft (7.6 m) and 45 ft (13.7 m) and utilize either two or three modules with spans between the interior columns of 50 ft (15.2 m) and 100 ft (30.4 m). The archetype buildings were designed and detailed by engineers at Metal Building Manufacturers Association (MBMA) member companies using their own internal design, detailing, and optimization software with the parameters defined in Table 1 and Table 2.

To ensure more sections of the frames are controlled by seismic demand, snow load combinations were not included in developing the frame designs because this leads to lower-weight design [see Moen et al. (2019) for influence of snow loads on seismic designs]. To ensure realistic secondary member sizes and eliminate site specificity, roof purlins, roof decks, diaphragms, girts, and lateral braces were designed against the U.S. average wind load for components and cladding, which corresponds to a wind speed of 110 mph (177 kph), assuming wind exposure category B (ASCE, 2016); however, wind did not control design of the frame members (i.e., seismic controls the lateral demands). The modular archetype metal buildings are designed for the design earthquake (DE) per ASCE 7-16 (2016). The values taken for the spectral response acceleration parameter at short period, S_s, and for the spectral response acceleration parameter at a period of 1.0, S_1, are based on recommendations provided in FEMA P695 (ATC, 2009).

NUMERICAL MODELING

This section describes the high-fidelity (primarily shell) finite element model used to predict the nonlinear lateral response of a modular metal building frame. The frame columns and rafters as well as the purlins, girts, and sheeting are all modeled with shell finite elements (Figure 3). Therefore, the model is capable of capturing local and global buckling of the rafters and columns; local, distortional, and

global buckling (including stiffness loss) of the purlins and girts; as well as buckling and yielding of the panel zone. The model does not include consideration of fracture. The initial modeling protocols, as detailed further below in their current use, were developed for the study on clear-span metal building frames (Meimand et al., 2018; Moen et al., 2019) and subject to peer review (see the Acknowledgments for the peer review team details). The main frame (rafter) modeling was validated against quasi-static cyclic frame subassembly tests conducted using AISC 341-10, *Seismic Provisions for Structural Steel Buildings* (2010), protocol (Smith et al., 2013). The complete model was validated against three full-scale shake table tests conducted at UCSD (Uang et al., 2011; Smith et al., 2013).

All finite element modeling in this study is performed in ABAQUS (Simulia, 2014). Model generation was automated using MathWorks (2018) to get all geometrical and material properties of the archetypes and generate ABAQUS input files. The inputs include rafter and column sizes, tapering, purlin and girt shapes, roof and wall panel sizes, main frame lateral bracing, lateral rod bracing, horizontal roof truss diaphragm, and the material properties of all associated parts.

The main frame is modeled with four-node S4R finite strain shell elements in ABAQUS, following mesh density guidelines defined in Schafer et al. (2010), which set a minimum of four nodes per local buckling half-wavelength. The plate-to-plate connections at the web-to-flange juncture or stiffeners to other elements are provided by common nodes, or tie constraints, and the welds are not explicitly modeled herein.

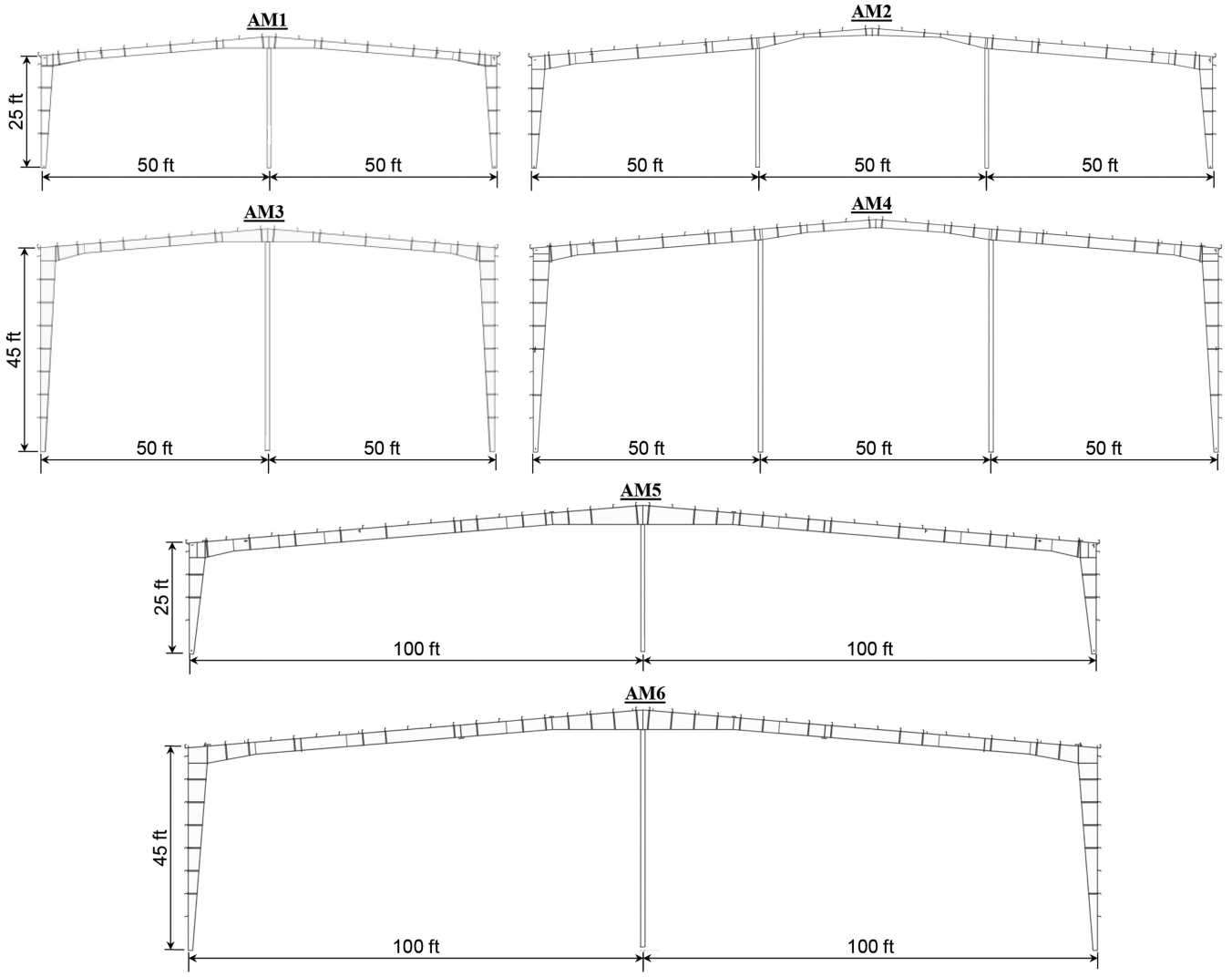

Fig. 2. Schematic elevation view of modular archetype buildings.

Table 2. Archetype Design Assumptions	
Summary of Demand Side (ASCE 7) Design Assumptions	
Building risk/occupancy category	II
Roof slope	1:12
Roof dead load [psf (Pa)]	2.2 (105.3)
Self-weight [psf (Pa)]	2.5 (119.7)
Collateral load [psf (Pa)]	7 (335.2)
Roof live [reducible) (psf (Pa)]	20 (957.6)
Snow load [psf (Pa)]	0 (0)
Rain load [psf (Pa)]	0 (0)
Wind speed [mph (kph)]	110 (177)
Wind exposure category	B
Seismic importance factor	1.0
Seismic design category	D
Site class	D
F_a, F_v	1, 1.7
S_s (g), S_1 (g)	1.5, 0.6
S_{DS}, S_{D1}	1, 0.68
R, Ω_o, C_d	3.5, 2.5, 3
Redundancy factor (ρ)	1.3
Design method	Allowable stress design
Seismic load	Equivalent lateral force procedure
Drift limit	No limit. Exterior walls accommodate frame drift (ASCE 7, Table 12.12-1, footnote c)
Summary of Capacity Side (AISC 360) Design Assumptions	
Metal building frame seismic detailing specifications	OMF
	Three-plate members; pinned base; no restriction on member compactness; no restriction on member splice locations; no restrictions on taper, pinch point, belly points; no special design of the panel zone
AISC 341 *Seismic Provisions*: overstrength conditions	AISC Design Guide 16 connection type, design knee connection with $R = 1.0$
	Use Ω_o forces only for column and base plate axial load, including anchor rods and welding.
Material	Specified $F_y = 55$ ksi (379 MPa), $F_u = 70$ ksi (482 MPa)
Welding	AWS D1.8 provisions, no protected zones
Anchor rods	ASTM F1554 A36

The pretensioned bolts of the end plate connections are not explicitly modeled, but the rafter (or column) end plate and the knee end plate are modeled to always stay in contact, assuming that the precompression is not overcome during the simulations.

The imperfections are considered as distortional buckling half-wavelength with the maximum web imperfection of $\delta = h/250$, where h is the depth of the web, as shown in Figure 4(a). A global out-of-plane sweep in the main frame span of $L/1000$ is also included based on measurements taken in the UCSD cyclic subassembly tests (Smith, 2013).

Thermal self-equilibrating residual stresses are modeled in the main frames with the stress distributions shown in Figure 4(b). The stress magnitudes are chosen based on the suggestions from Prawel and colleagues (1974) and Kim (2010) for built-up steel members.

Purlins and girts are also modeled using S4R shell elements, with a cross-section node pattern extruded along the length. The purlins are connected to the main frames with numerical constraints that link a group of nodes in the web and the bottom flange of the secondary member to a group of nodes on the main frame flange. These constraints approximate a typical clip connection. The girts and purlins are connected to the wall and roof panels by fasteners, where the fastener connection is modeled as a rigid constraint between coincident nodes using the MPC beam

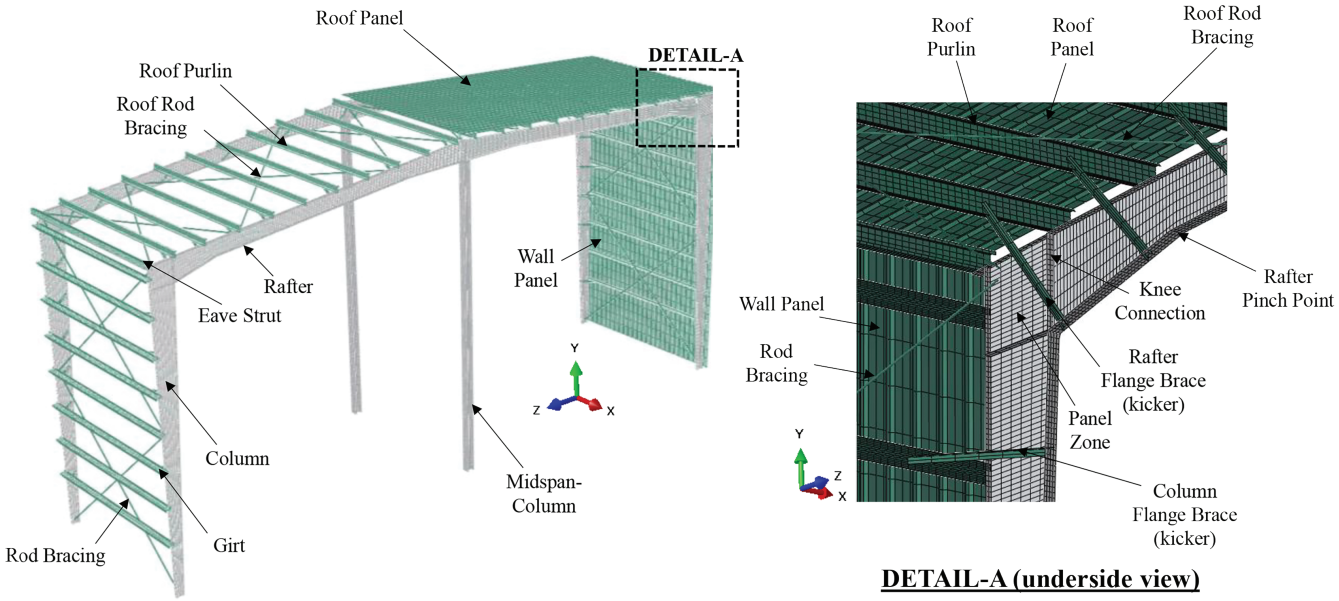

Fig. 3. High-fidelity finite element model.

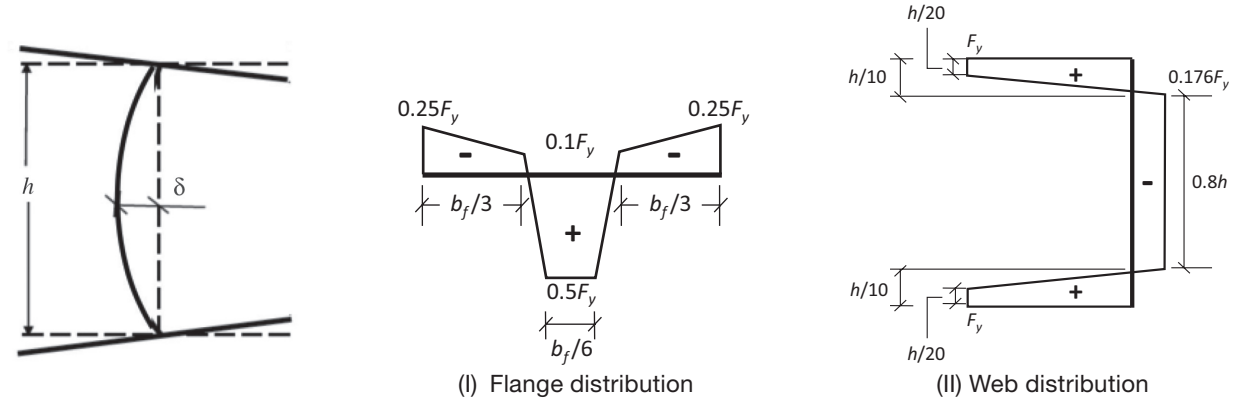

(a) Cross-sectional geometric imperfection pattern

(b) Thermal residual stress pattern (Kim, 2010)

Fig. 4. Mainframe cross-sectional geometric imperfection pattern and thermal residual stress pattern.

in ABAQUS. Initial geometric imperfections and residual stresses from manufacturing are not considered for any secondary members.

Rod braces are modeled with B33 beam elements in ABAQUS, and multi-point constraint (MPC) connections are used on the web near the top flange. The brace angle cross sections are modeled with S4R shell elements, and the brace ends are numerically constrained to node groups in the main frame flange and the purlin.

Wall and roof steel deck sheathing are modeled using shell elements, where sidelaps and endlaps are assumed to be continuous. Screw-fastened roofs are evaluated in this study, and each panel-to-purlin and panel-to-girt screw connection is modeled with a single-node rigid MPC.

Yield stress of 55 ksi (379 MPa) and ultimate stress of 70 ksi (482 MPa) are used for all steel structural elements. An isotropic-kinematic plasticity model, where the von Mises yield surface both expands and shifts to include residual stresses that remain after elastic unloading (i.e., the Bauschinger effect), is considered in both static and cyclic models. All secondary structural elements, including purlins, girts, and lateral braces, have a yield stress of 50 ksi (345 MPa) and an engineering strain hardening slope of 0.25% with isotropic hardening, where E is the elastic modulus of the steel material.

The base of the main frame columns was modeled as pinned, consistent with typical anchor rod and baseplate details in metal building systems. To check this assumption, the nonlinear spring model developed in Moen et al. (2019) was implemented for archetype AM2 with and without degradation, and the resulting ductility and overstrength values were found to be similar to those obtained using the pinned-base model.

ANALYSIS AND EVALUATION OF ARCHETYPE BUILDINGS

Pushover Analysis

Prior to performing nonlinear cyclic or dynamic analyses, a pushover analysis of the high-fidelity metal building model is performed. This analysis is utilized to determine the period-based ductility parameter (μ_T) and the system overstrength factor (Ω_o) for each archetype per FEMA P695. Additionally, the pushover analysis helps check the accuracy of the model and identify the expected failure modes. The pushover response also aids in defining a drift-based collapse limit, as detailed later in the Incremental Dynamic Analysis section. The model is fully geometric and material nonlinear and therefore includes all large deformation (P-Δ and P-δ) effects.

Figure 5 provides the static pushover response in terms of base shear versus roof displacement for all archetype buildings. "Tall buildings" AM3 and AM4 have insufficient ductility for successful seismic performance. Both suffer greater than 20% strength loss at peak load, although they have sufficient strength (i.e., the peak strength is well in excess of the design strength). The observed post-peak response for AM3 and AM4 are provided in Figures 5 and 6(a) and (c), respectively, and in both cases, one can observe that the girts are unable to brace the column rafter and that LTB in the column is occurring across multiple brace points. Consultation with the design engineers resulting in learning that the purlin and girt designs for AM3 and AM4 followed historical practice of using 2% of the compressive force (or flange force) in sizing the brace. AISC 360, Appendix 6, requires that both strength (often less than 2%) and stiffness be supplied by the bracing system. In this case, a redesign was required using heavier (thicker) girts to meet the stiffness requirement.

The performance of the redesigned AM3 and AM4 archetypes, designated as AM3R and AM4R, are provided in Figures 5 and 6(b) and (d). The overall response of the redesigned AM3R and AM4R results in adequate post-peak ductility and moves the limit state from LTB in the column to local buckling and yielding in the rafter. AM6 (the final tall building) was designed after AM3R and AM4R and also had the bracing provisions of AISC 360, Appendix 6 applied in its design. Note, AM1, AM2, and AM5 (the shorter buildings) did not have the AISC 360, Appendix 6 bracing provisions applied; however, they still performed well. Figure 5 provides the pushover response, and Figure 7 provides the deformed shape and stress contours for AM1, AM2, and AM5. The initial limit state is rafter yielding and local buckling at the haunch, and detrimental column LTB does not occur until larger drifts. It is anticipated that similar strength but improved post-peak performance is possible in these archetypes if they were to be redesigned to AISC 360, Appendix 6 bracing stiffness and strength provisions; however, given the performance was adequate as designed, the investigation of the overall performance proceeded without redesign and reanalysis on these archetypes.

Based on the nonlinear static pushover response, the resulting system overstrength (Ω_o), ductility (μ), and period-based ductility (μ_T) for each archetype are summarized in Table 3. The system overstrength is defined as:

$$\Omega_o = V_{max}/V_{design} \tag{1}$$

where V_{max} is the maximum base shear and V_{design} is the design base shear—that is, the lateral demand at the design earthquake (DE) level calculated using the ASCE 7-16 fundamental period, T_{ASCE7}. The ductility is defined as

$$\mu = \delta_u/\delta_y \tag{2}$$

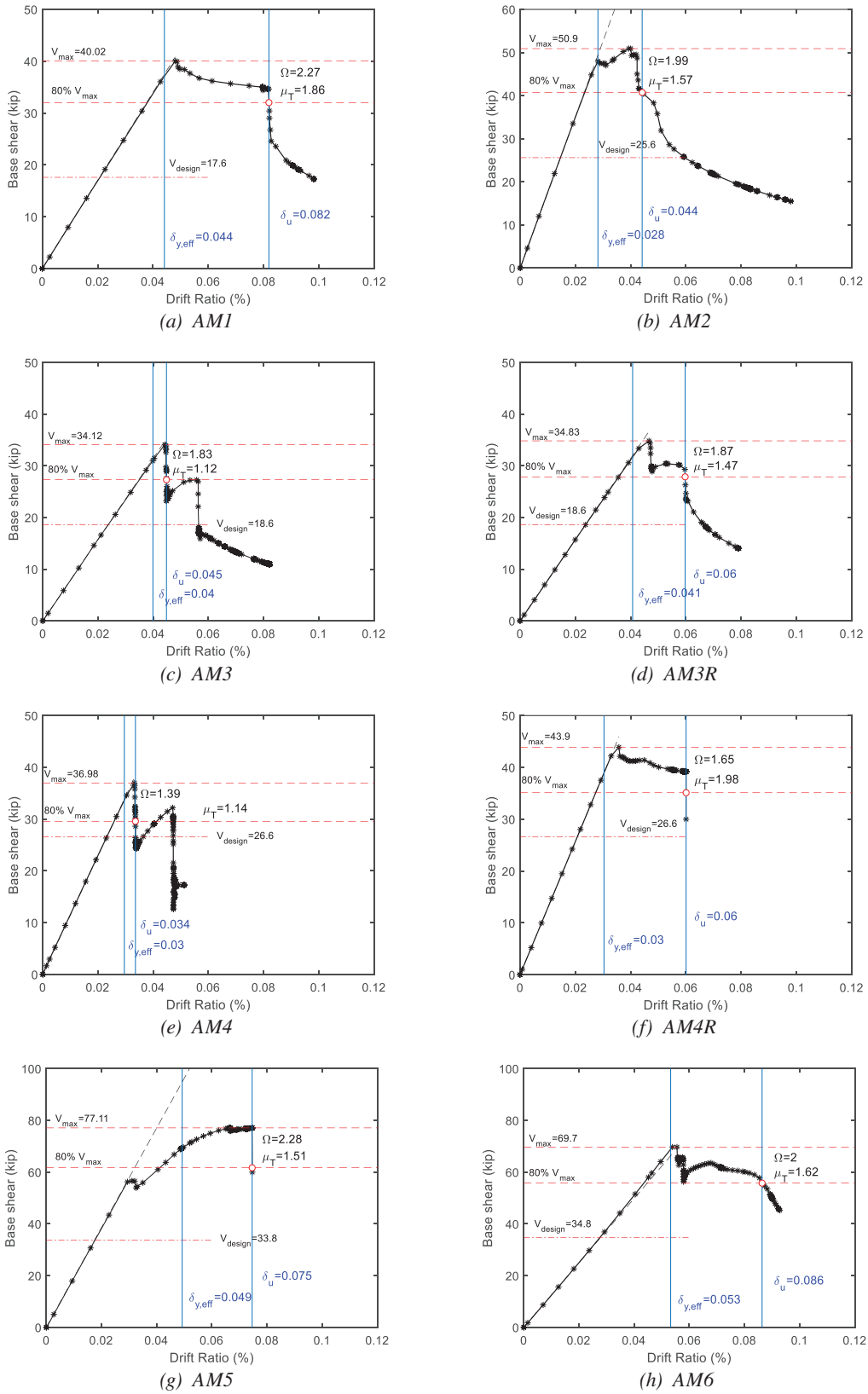

Fig. 5. Static pushover curve of archetypes (1 kip = 4.448 kN).

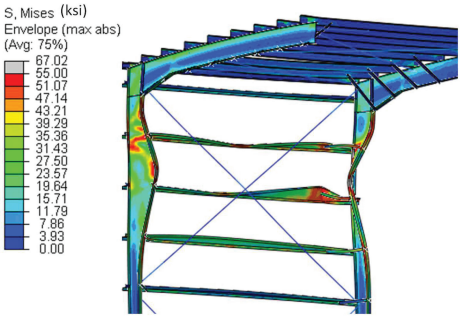

(a) AM3: 4.5% drift ratio

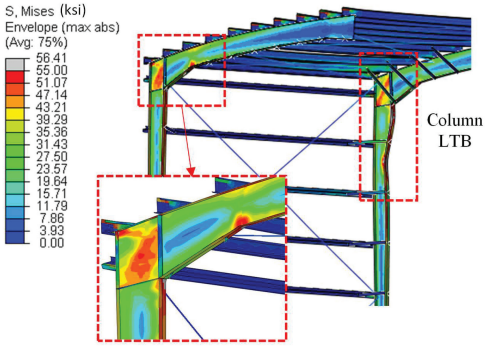

(b) AM3R: 4.7% drift ratio

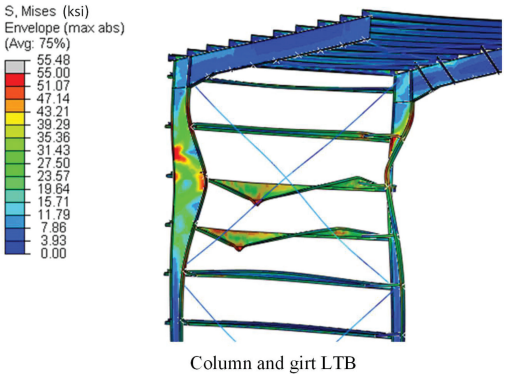

(c) AM4: 3.4% drift ratio

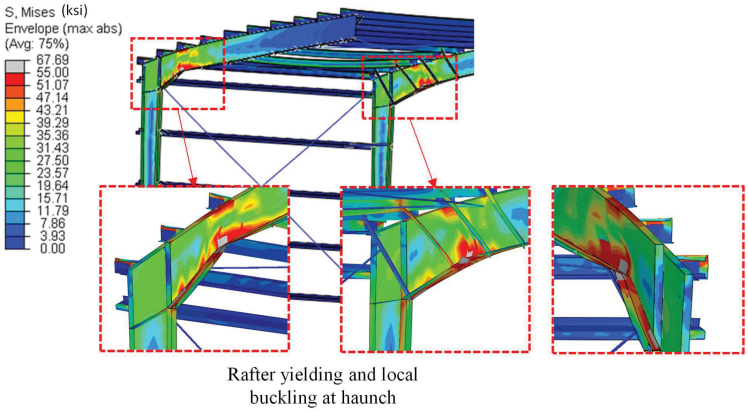

(d) AM4R: 3.6% drift ratio

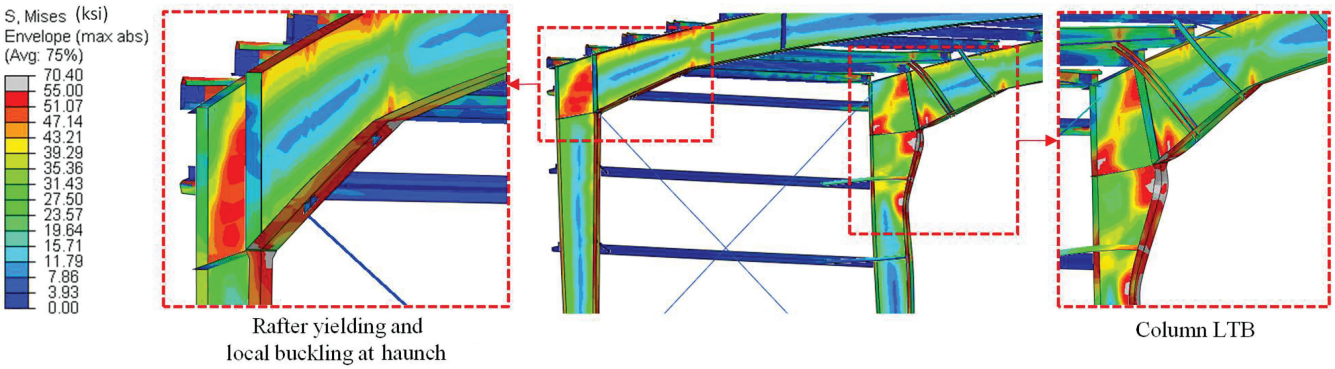

(e) AM6: 5.6% drift ratio

Fig. 6. First failure mode in tall buildings [45 ft (13.72 m)] (1 ksi = 6.895 MPa).

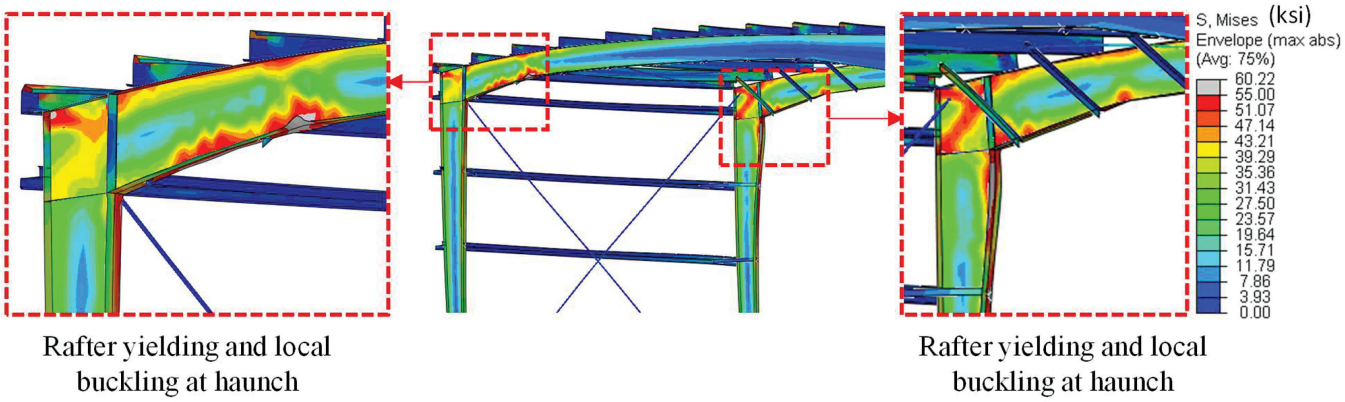

(a) AM1: 4.9% drift ratio

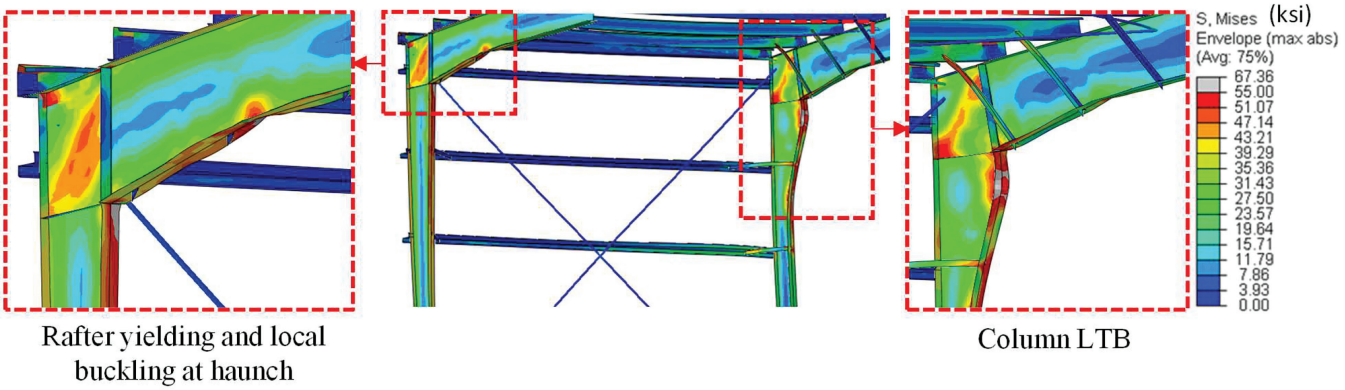

(b) AM2: 3.0% drift ratio

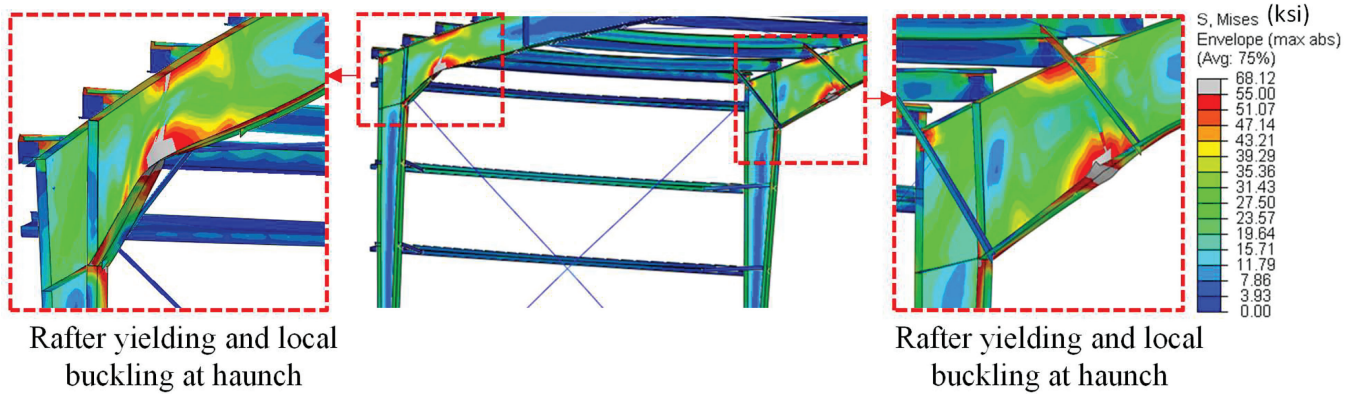

(c) AM5: 3.3% drift ratio

Fig. 7. First failure mode in short buildings [25 ft (7.62 m)] (1 ksi = 6.895 Mpa)

Table 3. Summary of System Overstrength (Ω_o), Ductility, and Period-Based Ductility (μ_T) Factors for Each Archetype.			
Archetype	**Overstrength**	**Ductility**	**Period-Based Ductility**
	Ω_o	μ	μ_T
AM1	2.27	1.67	1.86
AM2	1.99	1.49	1.57
AM3R	1.87	1.39	1.47
AM4R	1.65	>1.94*	>1.98*
AM5	2.28	>1.48*	>1.51*
AM6	2.00	1.47	1.62
Average	2.01	>1.57	>1.67
Archetypes Prior to Redesign of Bracing Stiffness per AISC 360			
AM3	1.83	1.07	1.12
AM4	1.39	1.09	1.14
* ">" indicates that the structure did not exhibit a 20% post-peak strength loss in the pushover analysis; the value is based on the last converged step and represents a conservative lower bound.			

Table 4. Sequence of Observed Behavior in Each Archetype						
	Observed Behavior					
Archetype	**Drift (%)**	**First Significant Behavior**	**Drift (%)**	**Second Significant Behavior**	**Drift (%)**	**Third Significant Behavior**
AM1	4.9	Rafter Y and LB	5.1	Rafter and column LTB	8.0	Rafter and PZ Y
AM2	3.0	Rafter Y and LB Column LTB	4.2	Rafter and PZ Y	4.3	Column LTB
AM3R	4.7	Rafter Y and LB Column LTB	4.7	Column LTB	5.8	Rafter and PZ Y
AM4R	3.6	Rafter Y, LB, and LTB	3.8	Rafter LTB and purlin LB	6.0	Rafter and PZ Y
AM5	3.3	Rafter Y, LB, and LTB	4.9	Rafter and PZ Y	6.7	Purlin LTB
AM6	5.6	Rafter Y and LB Column LTB	5.8	Rafter and purlin LTB	6.8	Rafter and PZ Y
Archetypes Prior to Redesign of Bracing Stiffness per AISC 360						
AM3	4.5	Column and girt LTB	5.6	Rafter and PZ Y	5.6	Column LTB
AM4	3.3	Column LTB	3.4	Girt LTB	4.7	Rafter Y Column LB and LTB
Note: Y: yielding, LB: local buckling, LTB: lateral-torsional buckling, PZ: panel zone						

Table 5. Summary of the Modal Analysis Results of the High-Fidelity Models and Period Evaluation of the Archetype Buildings per ASCE 7-16 Method

Archetype	Mass Participation Ratio	T_1 (s)	T_{ASCE7} (s)	T_{Design} (s)	$\frac{T_1}{T_{ASCE7}}$	$\frac{T_1}{T_{Design}}$
AM1	0.92	1.44	0.39	1.42	3.67	1.02
AM2	0.99	1.19	0.40	1.20	2.95	0.99
AM3R	0.96	2.02	0.61	1.98	3.31	1.02
AM4R	0.97	1.89	0.62	1.89	3.05	1.01
AM5	0.74	1.53	0.42	1.35	3.67	1.13
AM6	0.93	2.39	0.63	2.24	3.79	1.07

T_1: First period of high-fidelity shell finite element model
T_{ASCE7}: Estimate period based on ASCE 7-16, Equation 12.8-7 (ASCE, 2016)
T_{Design}: Period estimate by metal building designer based on beam element approximation

where δ_u is the ultimate roof drift displacement—that is, the roof displacement at $0.8V_{max}$—and δ_y is the yield roof drift displacement, defined as

$$\delta_y = V_{max}/k_e \tag{3}$$

where k_e is the initial (elastic) stiffness of the building. The period-based ductility is defined as

$$\mu_T = \delta_u/\delta_{y,eff} \tag{4}$$

where δ_u is the ultimate roof drift—that is, the roof displacement at $0.8V_{max}$—and $\delta_{y,eff}$ is the effective yield roof drift displacement, defined in FEMA P695 as:

$$\delta_{y,eff} = C_o\left(\frac{V_{max}}{W}\right)\left(\frac{g}{4\pi^2}\right)\left[max(T, T_1)\right]^2 \tag{5}$$

where T is the fundamental period per ASCE 7-16, T_1 is the fundamental period of the building models computed using eigenvalue analysis (see Frequency Analysis section), W is the seismic weight of the building, g is the acceleration of gravity, V_{max} is the maximum base shear of the building, and C_o is the modal coefficient (which is 1.0 for a single-story structure like a metal building).

According to Table 3, the calculated overstrength factors are in the range of 1.6 to 2.3. According to the FEMA P695 procedures, the system overstrength, Ω_o, is calculated as the maximum of the average from the different performance groups, but not to exceed a maximum value of Ω_o = 3.0. Accordingly, from the archetype analysis summarized in Table 3, the design value would be set to Ω_o = 2.0, governed by the average value of the performance group.

The nonlinear static pushover analysis provides a clear examination of the expected limit states. The sequence of failure modes observed in each archetype is presented in Table 4.

Major observations from the nonlinear static response include the following:

- In "short" archetypes [H = 25 ft (7.62 m)] AM1, AM2, and AM5, the post-peak response is primarily dominated by rafter yielding and local buckling at the haunch, followed by rafter span LTB at larger drift ratios in all three archetypes and minor column LTB in AM1 and AM2.
- In tall archetypes [45 ft (13.72 m)] with column lateral bracing designed per the strength-only (2%) method (i.e., AM3 and AM4), the post-peak strength degradation is dominated by severe column LTB [Figures 6(a) and (c)], followed by girt LTB due to the diagonal brace (kicker) force at the location of column lateral braces. The high sensitivity of AM3 and AM4 to column LTB results in significantly lower ductility than the other archetypes. These bracing designs do not meet the criteria of AISC 360.
- In tall archetypes with column lateral bracing designed per AISC 360 (AM3R, AM4R, and AM6), the post-peak strength degradation is primarily dominated by rafter yielding and local buckling at the haunch followed by rafter span or minor column LTB [Figures 6(b), (d), and (e)]. The lower sensitivity of AM3R, AM4R, and AM6 to column LTB results in a more stable post-peak response and higher ductility than AM3 and AM4.

With these findings, it was concluded that application of the OMF criteria in seismic design of metal buildings must adhere to all provisions of AISC 360, including the bracing provisions, and that the design of braces for 2% of the compressive force is not sufficient. Therefore, further analysis would only be conducted on AM3R and AM4R. As a result, in the analyses that follows AM3 and AM4 are replaced by AM3R and AM4R.

Frequency (Modal) Analysis

The natural periods and mass participation of the modular metal building archetypes are provided in Table 5. The natural period of the tall archetypes (AM3R, AM4R, and AM6) is between 2.02 and 2.39 s, while that of the shorter ones (AM1, AM2, and AM5) ranges from 1.19 to 1.89 s. The high-fidelity model and the beam element model used in the design agree strongly, while the empirical equations in ASCE 7-10 (ASCE, 2010) were found to assume far stiffer response than is typically realized in metal building frames.

Cyclic Analysis

The high-fidelity models are used to characterize the quasi-static cyclic response of the archetypes, including strength and stiffness degradation. Each archetype metal building is subjected to cyclic horizontal displacements per AISC 341 cyclic loading protocol at the knee level. The cyclic response is defined as the base shear versus drift ratio in Figure 8. The cyclic results generally follow the pushover backbone, but some minor cyclic degradation is observed in the archetypes. The quasi-static cyclic behavior is used to calibrate a nonlinear single-degree-of-freedom (SDOF) model utilized in incremental dynamic analysis and discussed in the following section.

Incremental Dynamic Analysis

The objective of the nonlinear incremental dynamic analysis (IDA) is to determine the ground motion intensity corresponding to the collapse of the structure, per the FEMA P695 procedure. A collapse limit (e.g., drift limit) is required in the IDA procedure to estimate the probability of collapse and determine the acceptability of the seismic response modification coefficients utilized in design. Selection of the collapse limit for the modular metal buildings requires some care. In the available full-scale (clear-span) metal building shake table tests (Uang et al., 2011; Smith, 2013), collapse was not observed up to 4% story drift, so a direct experimental collapse drift limit is unavailable. Moen et al. (2019) utilized a 4.5% collapse drift limit in their modeling, based on the observation that plastic strain accumulation in the rafter and panel zone would eventually lead to fracture (which was not included in the model). Modular metal building systems are flexible. Review of the pushover response of Figure 5 indicates that most of the archetypes are in the elastic or initial post-yield hardening response at 4.5% drift; therefore, such a limit for collapse would be inappropriate. An archetype-dependent collapse drift limit is possible; however, a simpler approach was selected here—the collapse drift limit was assumed to be 6% for modular metal buildings. In all archetypes, except for AM2, the ultimate drift ratio (drift ratio corresponding to 20% strength loss) is greater than 6%. Plastic strain accumulation does not initiate until the first significant nonlinear response is observed, which is generally greater than 4%; thus, the use of 6% recognizes the inherent flexibility of the modular metal building archetype but still limits the total plastic strain accumulation in the response.

A set of 22 pairs of ground motions (44 total) specified in Appendix A of FEMA P695 were used for the IDA. The IDA procedure starts by defining the median spectral intensity of the far-field record set, S_T, measured at the fundamental period of the structure, and then the far-field record set is scaled by $\alpha = S_{MT}/S_T$, where α is the intensity factor and S_{MT} is the spectral intensity corresponding to the maximum considered earthquake (MCE) at the fundamental period of the structure. The median collapse intensity corresponding to the spectral acceleration at the fundamental period of the building at which half of the ground motions cause collapse is referred to as $\hat{S}_{CT}$. IDAs are performed using the nonlinear SDOF modeling protocol introduced in the following section.

Computationally Efficient Nonlinear Dynamic Analysis Framework

The dynamic behavior of metal buildings, as a single-story moment frame with roof masses, can be represented by a single-degree-of-freedom (SDOF) dynamic system. The first mode mass participation ratio of previously studied clear-span metal buildings is between 76% and 83% (Moen et al., 2019). The first mode mass participation ratio of the modular metal building archetypes with 50 ft (15.2 m) modules (AM1–AM4R) are between 92% and 99% per Table 5. The longer span 100 ft (30.4 m) modules of AM5 and AM6 have lower mass participation ratios, 74% and 93%, respectively. The long rafter spans and short columns of AM5 are indicative of the potential for some higher mode response in this specific archetype; however, the nonlinear static response and observed failure mechanism is benign in this archetype as indicated by its high overstrength and ductility (see Figure 5 and Table 3), and the lower mass participation ratio for this archetype was deemed acceptable for the study.

A classical SDOF dynamic model can be represented by a lumped mass, m, spring stiffness, K_t, and damping, c, as shown in Figure 9. The dynamic properties—specifically, the period of vibration, T—can be selected so the SDOF model is consistent with what would be expected for the actual building. Strength and stiffness degradation and the period shift as the building experiences damage during an earthquake are approximated by the nonlinear spring stiffness, K_t. A SDOF hysteretic material model may be matched to the cyclic hysteretic response of the high-fidelity model. With this high-fidelity to SDOF mapping, the SDOF cyclic response includes local and system-level responses,

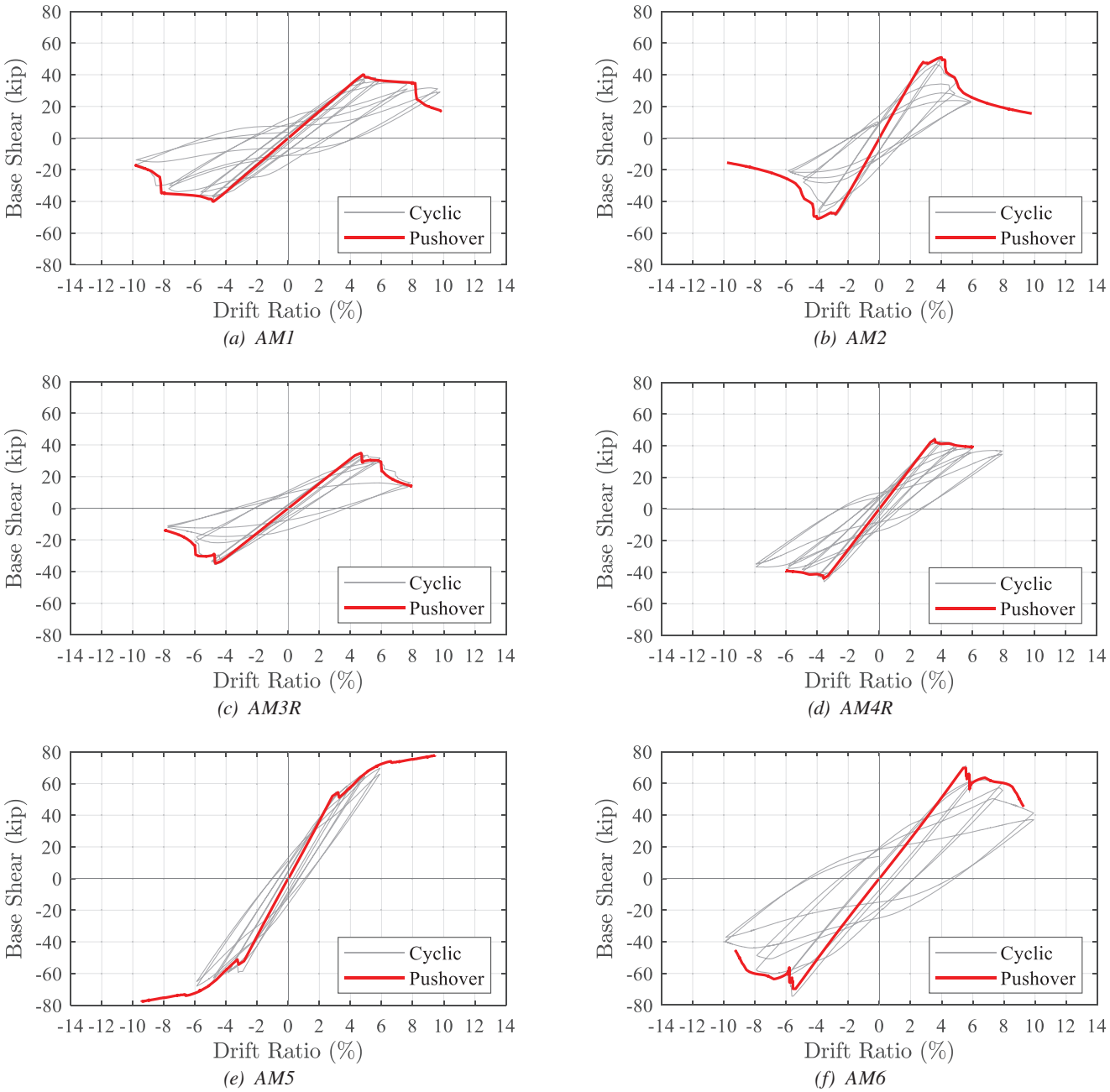

Fig. 8. Quasi-cyclic and pushover response of archetypes (1 kip = 4.448 kN).

including rafter lateral-torsional buckling and local buckling and bracing from the secondary structural system (purlins, girts, kickers, etc.).

The Pinching 04 material model in OpenSees is utilized for the nonlinear SDOF material hysteretic model. The Pinching 04 model includes the definition of four response points as illustrated in Figure 10 and additional parameters to handle loading/unloading (pinching) and cyclic degradation. Here, the backbone points and other parameters are established such that the per-cycle and accumulated error between the SDOF model and the high-fidelity model response are minimized, as illustrated for AM2 in Figure 11. This process is repeated for all studied archetypes. The Pinching 04 model fitting parameters for all archetypes are presented in Appendix Table A.

The seismic mass, m, is assumed to be equal to the mass used to calculate the design seismic weight in an equivalent lateral force procedure. Matching the fundamental building period to the SDOF model is desirable so that elastic behavior and the natural periods are consistent. The relationship among the mass, initial stiffness, and period of the building can be written as follows:

$$T_1 = 2\pi\sqrt{m/k_i} \tag{6}$$

where m is the seismic mass, k_i is the initial stiffness of the building in the SDOF model, and T_1 is the fundamental period of the SDOF model. Because the building period is determined by high-fidelity analysis, and the seismic mass

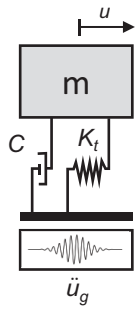

Fig. 9. Metal building nonlinear SDOF model definitions.

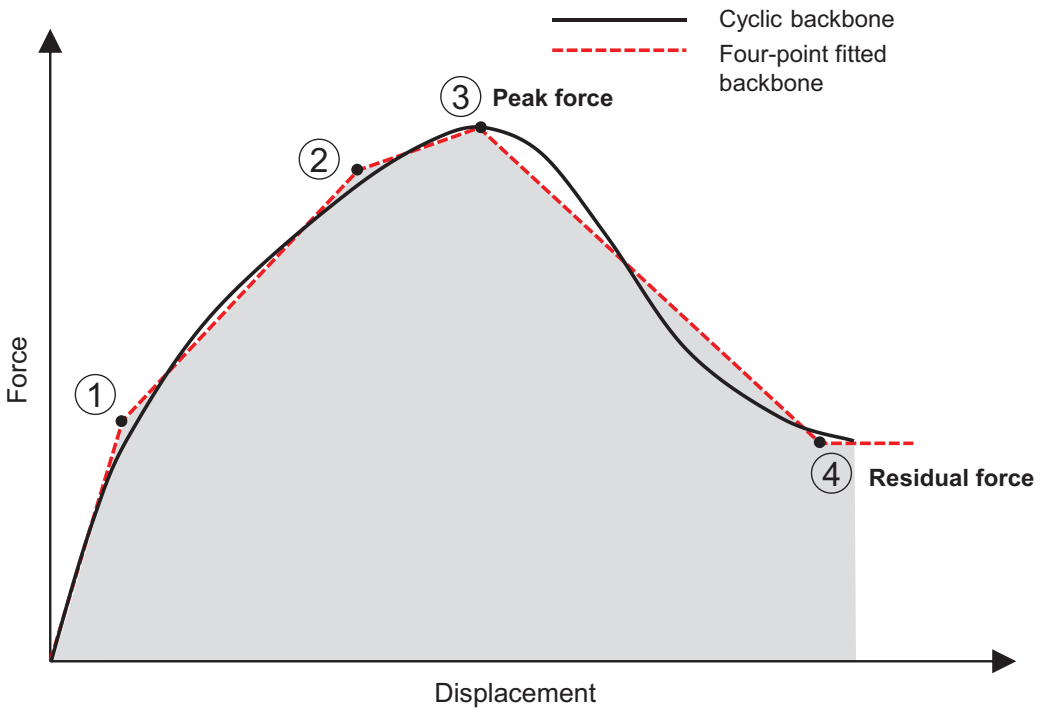

Fig. 10. A four-point backbone fitted to the cyclic backbone is shown in the first quadrant.

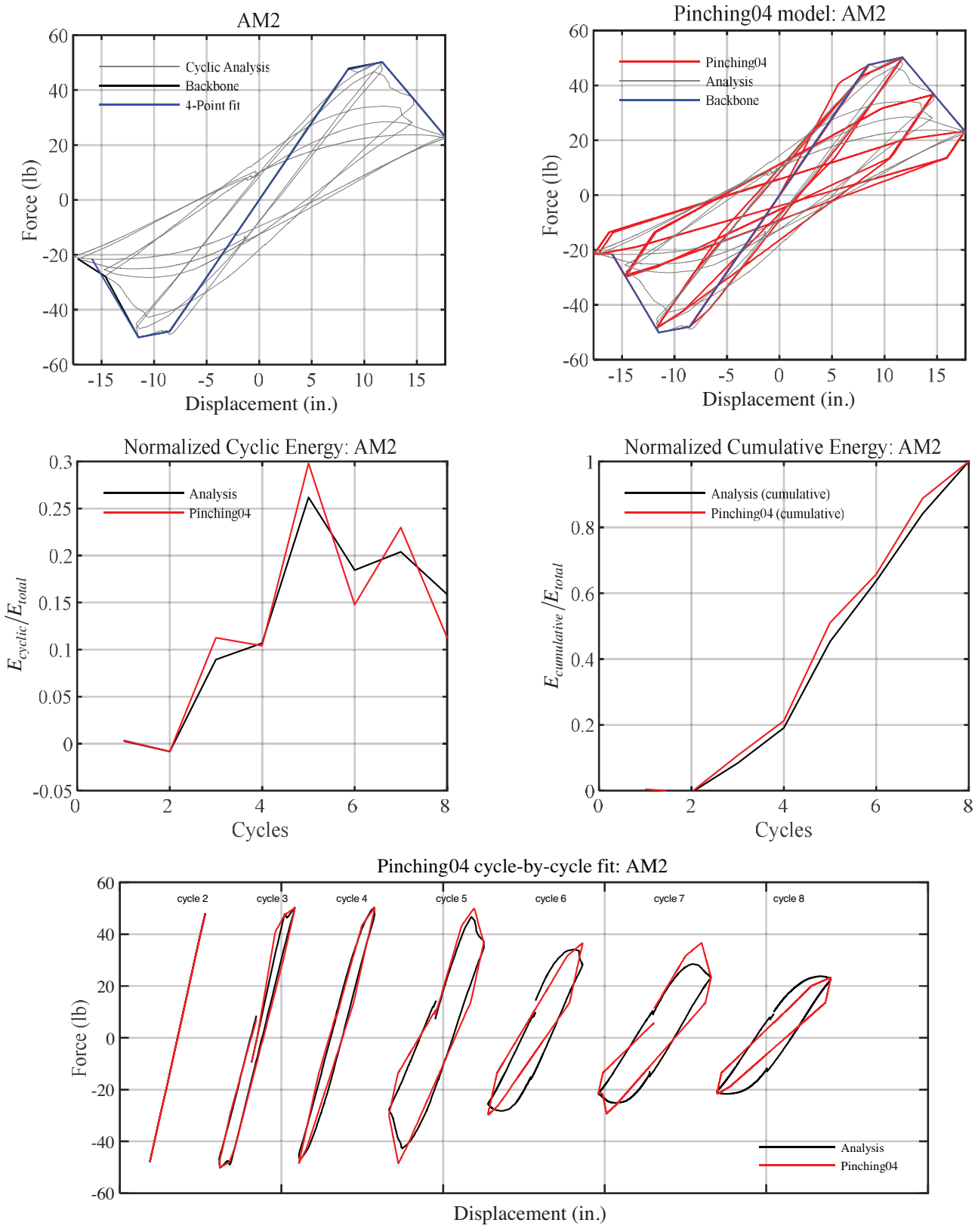

Fig. 11. Quasi-static cyclic response of AM2: High-fidelity simulation and fitted response using Pinching 04 hysteretic model in OpenSees (McKenna et al., 2004) (1 kip = 4.448 kN; 1 in. = 25.4 mm).

Table 6. Summary of Archetypes Analyses Results: Collapse Drift Limit of 6% ($R = 3.5$, $\Omega_o = 3$, $C_d = 3$)										
Archetype	Ω_o	μ_T	S_{CT} (g)	SMT (g)	*CMR*	*SSF*	*ACMR*	$ACMR_{10\%}$	$ACMR_{20\%}$	Check (Pass/Fail)
AM1	2.27	1.86	0.80	0.63	1.28	1.21	1.54	1.70	1.42	Pass
AM2	1.99	1.57	0.99	0.76	1.31	1.16	1.52	1.66	1.39	Pass
AM3R	1.87	1.47	0.79	0.45	1.78	1.16	2.07	1.65	1.39	Pass
AM4R	1.65	>1.98	0.85	0.48	1.79	1.23	2.20	1.72	1.43	Pass
AM5	2.28	>1.51	0.75	0.59	1.27	1.17	1.48	1.65	1.39	Pass
AM6	2.00	1.62	0.54	0.38	1.43	1.18	1.69	1.67	1.40	Pass
						Average	1.75	1.67	—	Pass

of the building is also defined in the seismic design of the building, an equivalent initial stiffness is required to match the actual building period to the SDOF model. Chapter 6 of FEMA P695 (ATC, 2009) addresses this challenge by defining an effective yield roof drift displacement, $\delta_{y,eff}$, as defined in Equation 5. For a single-story structure like a metal building, the modal coefficient C_o is 1.0, and by assuming that the actual period of the building is larger than the ASCE 7 (2010) prediction ($T_1 > T$), Equation 5 can be simplified to

$$V_{\max}/\delta_{y,eff} = 4\pi^2 m/T_1^2 \tag{7}$$

By further noting $k_{eq} = V_{max}/\delta_{y,eff}$, the equivalent initial stiffness for the SDOF model, k_{eq}, can be calculated as

$$k_{eq} = 4\pi^2 m/T_1^2 \tag{8}$$

This equivalent initial stiffness is used in the Pinching 04 models.

The last term to consider in the SDOF dynamic equation is energy dissipation treated with the viscous damping ratio, ξ. For all simulations in this study, $\xi = 2\%$ is selected, corresponding to a low-intensity elastic response, assuming that energy dissipation from yielding, buckling, and damage is accounted for in the hysteretic response.

IDA and Fragility Curves

Story-drift versus the earthquake spectral acceleration scale factor and the resulting fragility response for all archetypes are provided in Figures 12(I) and (II), respectively. As an example, for AM5, the median collapse capacity (from all 44 records) is $\hat{S}_{CT} = 0.75$ g [Figure 12(e) (II)], and the $CMR = \hat{S}_{CT}/S_{MT} = 0.75/0.59 = 1.27$. Collapse fragility curves are also used to express this information, where the cumulative collapse probability is related to the ground motion spectral intensity. The discrete points in Figure 12 are obtained directly from the collapse points of the IDA curve for each archetype. A lognormal distribution is fit to the data to get a smooth curve and obtain $\hat{S}_{CT}$.

Per FEMA P695, the fragility response should be modified with the spectral shape factor, *SSF*, to account for the spectral shape. The *SSF* is a function of the building fundamental period, *T*, and period-based ductility, μ_T, used to calculate the adjusted collapse margin ratio as $ACMR = SSF \times CMR$. For AM5, for example, $ACMR = 1.17 \times 1.27 = 1.48$. Similar results are provided for all studied archetypes in Table 6.

SEISMIC PERFORMANCE ASSESSMENT PER FEMA P695 METHODOLOGY

Per FEMA P695 (ATC, 2009), the performance of a system is judged by comparing the adjusted collapse margin ratios (ACMR) to the lower bound acceptable collapse margin ratios: $AMCR_{10}\%$ or $AMCR_{20}\%$ as specified in FEMA P695. The performance of a structural system is acceptable if, under the MCE ground motion, each archetype has a large enough collapse capacity such that the probability of collapse is less than 20% ($ACMR > ACMR_{20\%}$), and the performance group must, on average, have less than 10% probability of collapse ($\overline{ACMR} > ACMR_{10\%}$, where $\overline{ACMR}$ is the average ACMR of the performance group). The acceptable ACMRs are calculated by assuming the distribution of collapse level spectral intensities is lognormal, with a median equal to $\hat{S}_{CT}$, and a standard deviation of β_{TOT}, which represents the total uncertainty in the collapse behavior of the system calculated as

$$\beta_{TOT} = \sqrt{\beta_{RTR}^2 + \beta_{DR}^2 + \beta_{TD}^2 + \beta_{MDL}^2} \tag{9}$$

where β_{RTR} is the record-to-record collapse uncertainty defined as

$$\beta_{RTR} = 0.1 + 0.1\mu_T \le 0.4 \tag{10}$$

and β_{DR} reflects the uncertainty in the implementation of design and quality assurance requirements, β_{TD} demonstrates the uncertainty in the quality and completeness of

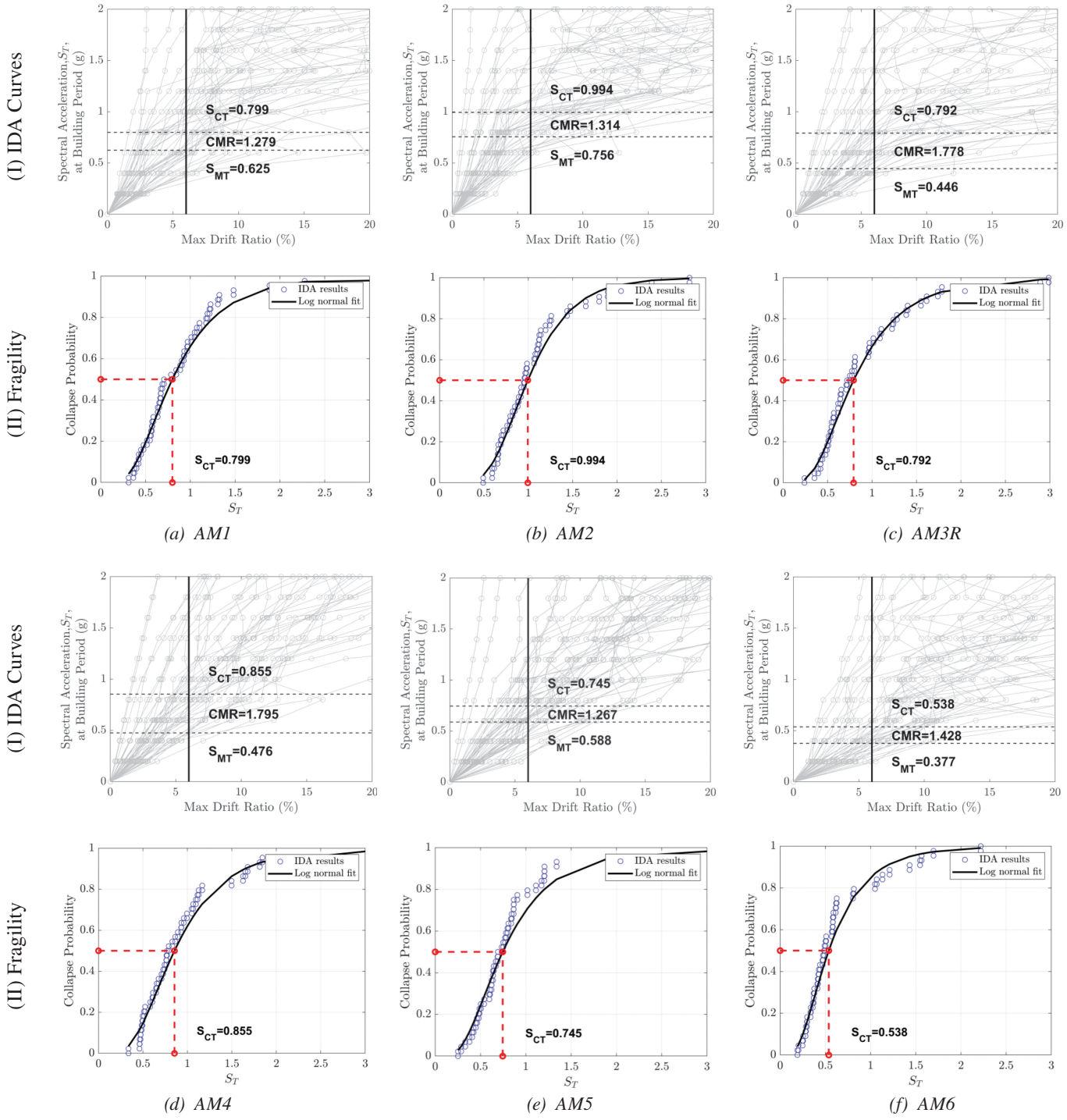

Fig. 12. IDA and fragility curves for archetypes.

the test data to characterize the structural behavior, and β_{MDL} reflects the uncertainty in the accuracy and variability of the structural modeling (ATC, 2009).

For the present study, β_{TOT} was defined using Equation 9, and the assumed uncertainties were $\beta_{DR} = 0.20$, $\beta_{TD} = 0.20$, and $\beta_{MDL} = 0.10$. β_{DR} is low because the archetype buildings are designed professionally, and the designs are reviewed internally and by the MBMA seismic steering group. The test data-related uncertainty β_{TD} is low since shake table test data are available for the underlying modeling protocol development. The modeling-related uncertainty β_{MDL} is low because collapse characteristics, including local and global buckling, are represented well in high-fidelity and nonlinear SDOF models.

The seismic response parameters, specifically, the median collapse intensity, $\hat{S}_{CT}$, the collapse margin ratio, *CMR*, the adjusted collapse margin ratio, *ACMR*, and acceptable collapse margin ratios ($ACMR_{10\%}$ and $ACMR_{20\%}$) are summarized in Table 6. The index archetypes meet the individual and group acceptance criteria. Thus, the assumed design seismic response modification factor R = 3.5 (Table 2) is deemed to satisfy the minimum acceptance criteria of FEMA P695 for modular metal buildings with two and three spans with different heights and span widths.

DISCUSSION

High-fidelity simulations coupled with surrogate models can provide an effective means for evaluating metal building system seismic performance. Conventional design processes provide acceptable outcomes in past experimental work and current P695-based modeling efforts but may still behave differently than expected by engineers. Drift is driven largely by LTB between and across brace points, not yielding. Modifying R in the initial design does not typically result in significantly different frame performance given the limited range in which lateral loads control the moment envelope and given that frames are fully optimized to that moment envelope. Lateral performance of the frames in modular metal buildings is not markedly different from clear-span buildings; however, they can be much more flexible. Innovative seismic systems and the necessity of the limits of current ASCE 7 code provisions (height, weight, etc.) could all now be efficiently explored using the developed models and protocols.

SUMMARY AND CONCLUSION

This study evaluated the seismic performance of modular metal buildings in high seismic zones using the FEMA P695 methodology. A representative set of archetype buildings, reflecting current industry design practices and incorporating ordinary moment frame (OMF) behavior with a response modification factor of R = 3.5, was developed and analyzed through modal analysis, nonlinear static pushover, quasi-static cyclic simulations, and incremental dynamic analyses (IDAs). High-fidelity finite element models, calibrated to experimental data from prior shake table and subassembly tests, were used to capture the nonlinear behavior of the archetypes and to provide an accurate assessment of collapse performance, with fracture not explicitly modeled. For the FEMA P695 evaluation, these high-fidelity models were further idealized into calibrated nonlinear single-degree-of-freedom (SDOF) systems, which formed the basis of the collapse assessment.

The results of this study confirm that modular metal buildings designed with R = 3.5 can meet the FEMA P695 acceptance criteria, provided that lateral bracing systems for both columns and rafters are designed to satisfy the strength and stiffness requirements of AISC 360, Appendix 6. In contrast, buildings designed with traditional strength-only (2%) bracing methods exhibited reduced ductility and early onset of lateral-torsional buckling (LTB) in columns, which significantly compromised ductility. Redesign of the lateral bracing to include adequate stiffness, in accordance with AISC provisions, resulted in improved post-peak behavior and increased system ductility.

The nonlinear static and dynamic analyses also showed that modular metal buildings remain largely elastic up to approximately 4% story drift and that ultimate drift ratios generally exceed 6%. Based on this observed performance, a collapse drift limit of 6% is proposed as more appropriate for modular metal buildings than the 4.5% previously adopted in studies of clear-span metal buildings for use within the FEMA P695 evaluation framework only, and not as a prescriptive limit for design practice. The calibrated SDOF models used in this study were able to effectively reproduce the cyclic and collapse behavior of the archetypes, enabling efficient implementation of the FEMA P695 framework.

Overall, the results confirm the applicability and adequacy of the ASCE 7 seismic design provisions where modular metal buildings are categorized as ordinary moment frames when modern bracing design practices are employed. The study highlights the importance of meeting both strength and stiffness criteria in lateral bracing systems and provides a technical foundation for the continued use of R = 3.5 in the seismic design of modular metal buildings, within the scope of modular metal buildings up to 45 ft (13.7 m) in eave height and with roof loads not exceeding 20 psf (0.96 kN/m²).

ACKNOWLEDGMENTS

The authors would like to thank the Metal Building Manufacturers Association (MBMA) Seismic Research Steering Group who provided thoughtful advice, input, effort, and

feedback throughout this project. In addition, several engineers in this group provided the complete designs for the metal building system archetypes. The authors would also like to thank the peer review panel, comprised of Dr. Greg Deierlein, Dr. Michael Engelhardt, and Dr. Tom Sabol, who reviewed the modeling protocols and conclusions in detail for the clear-span seismic study that preceded this work. In addition, Dr. Chia-Ming Uang was gracious with his time and data during the validation phase of the modeling. Finally, Dr. Lee Shoemaker and Mr. Vincent Sagan of MBMA were instrumental in shepherding this project to a meaningful end. The team would also like to recognize the financial support of MBMA in conducting the work.

REFERENCES

AISC (2010), *Seismic Provisions for Structural Steel Buildings*, AISC 341-10, American Institute of Steel Construction, Chicago, Ill.

AISC (2016), *Specification for Structural Steel Buildings*, ANSI/AISC 360-16, American Institute of Steel Construction, Chicago, Ill.

ASCE (2010), *Minimum Design Loads and Associated Criteria for Buildings and Other Structures*, ASCE/SEI 7-10, Reston, Va.

ASCE (2016), *Minimum Design Loads and Associated Criteria for Buildings and Other Structures*, ASCE/SEI 7-16, Reston, Va.

ATC (2009), *Quantification of Building Seismic Performance Factors*, FEMA P695, Federal Emergency Management Agency, Washington, D.C.

Bagatini Cachuço, F. (2021), "Seismic Performance Evaluation of Steel Building Systems in Canada," Master's Thesis, University of British Columbia, Vancouver, Canada.

Bagatini Cachuço, F. and Yang, T.Y. (2021), "Seismic Performance Assessment of Pre-Engineered Steel Buildings on the West Coast of Canada," *Steel and Composite Structures: An International Journal*, Vol. 41, No. 3, pp. 461–474, https://doi.org/10.12989/scs.2021.41.3.461.

Hong, J.K. and Uang, C.M. (2006), "Cyclic Performance Evaluation of a Metal Building System with Web-Tapered Members," Report No. SSRP-06, Department of Structural Engineering, University of California–San Diego, La Jolla, Calif.

Hatch, J. (2014, August), "New Advances in Design and Testing for Seismic Demands," *STRUCTURE Magazine*, https://www.structuremag.org/.

Kaehler, R.C., White, D.W., and Kim, Y.D. (2011), *Frame Design Using Web-Tapered Members*, Design Guide 25, AISC, Chicago, Ill.

Kim, Y.D. (2010), "Behavior and Design of Metal Building Frames with General Prismatic and Web-Tapered Steel I-Section Members," Doctoral Dissertation, Georgia Institute of Technology, Atlanta, Ga.

MathWorks (2018), The MathWorks, Inc., Natick, Mass., www.mathworks.com.

McKenna, F., Fenves, G.L., and Scott, M.H. (2004), "Open System for Earthquake Engineering Simulation," Pacific Earthquake Engineering Research Center, University of California–Berkeley, Berkeley, Calif.

Meimand, V., Moen, C., and Schafer, B. (2018), "Examination of Seismic Response Modification Coefficients for Metal Building Systems with FEMA P695 Process," in *Proceedings of the 11th National Conference on Earthquake Engineering (NCEE)*, Earthquake Engineering Research Institute, Los Angeles, Calif.

Moen, C.D., Torabian, S., and Schafer, B.W. (2019), "Evaluation of Metal Building System Seismic Response Modification Coefficients," Johns Hopkins University, https://jscholarship.library.jhu.edu/items/3fb18f3a-c7e9-4696-b32a-188fd336af76.

Prawel, S.P., Morrell, M.L., and Lee, G.C. (1974), "Bending and Buckling Strength of Tapered Structural Members," *Welding Research Supplement*, Vol. 53, No. 2, pp. 75–84.

Schafer, B.W., Li, Z., and Moen, C.D. (2010), "Computational Modeling of Cold-Formed Steel," *Thin-Walled Structures*, Vol. 48, No. 10–11, pp. 752–762, https://doi.org/10.1016/j.tws.2010.05.004.

Simulia (2014), ABAQUS (Version 6.14), Dassault Systèmes.

Smith, M.D. (2013), "Seismic Testing and Analytical Studies for the Development of New Seismic Force Resisting Systems for Metal Buildings," Doctoral Dissertation, University of California–San Diego, La Jolla, Calif.

Smith, M.D., Turner, K.T., and Uang, C.M. (2013), "Experimental Investigation of Cyclic Lateral Buckling of Web-Tapered I-Beams," Report No. SSRP-12, Department of Structural Engineering, University of California–San Diego, La Jolla, Calif.

Uang, C.M., Smith, M.D., and Shoemaker, W.L. (2011), "Earthquake Simulator Testing of Metal Building Systems," in *Structures Congress 2011*, pp. 693–704, American Society of Civil Engineers, Las Vegas, Nev., https://doi.org/10.1061/41171(401)62.

APPENDIX

Table A. Pinching 04 Model Parameters for All Archetypes							
		Archetype					
Parameter	**Unit**	**AM1**	**AM2**	**AM3R**	**AM4R**	**AM5**	**AM6**
ePf1	kips	23.6	29.4	17.4	27.1	41.8	43.2
ePd1	in.	8.6	5.2	12.2	11.4	6.9	18.4
ePf2	kips	31.6	47.4	30.6	36.1	58.5	56.5
ePd2	in.	11.6	8.4	21.6	15.2	10.9	24.0
ePf3	kips	39.4	50.2	35.1	45.1	69.7	71.1
ePd3	in.	14.6	11.7	25.5	19.3	17.7	30.0
ePf4	kips	31.2	23.3	16.0	36.7	50.0	41.4
ePd4	in.	26.7	17.6	43.6	35.3	20.0	54.7
eNf1	kips	–24.1	–26.3	–21.5	–29.4	–29.9	–44.7
eNd1	in.	–8.8	–4.7	–15.0	–12.3	–4.9	–18.9
eNf2	kips	–28.8	–48.0	–28.4	–35.6	–60.6	–56.0
eNd2	in.	–10.5	–8.6	–19.8	–15.0	–10.0	–23.7
eNf3	kips	–39.6	–50.1	–35.6	–46.0	–67.9	–74.4
eNd3	in.	–14.2	–11.5	–25.6	–19.2	–17.7	–30.4
eNf4	kips	–16.7	–21.5	–12.1	–36.6	–50.0	–39.9
eNd4	in.	–30.7	–15.9	–38.4	–32.6	–20.0	–53.8
rDispP	–	0.705	0.667	0.648	0.751	0.656	0.533
rForceP	–	0.917	0.863	0.857	0.834	0.757	0.979
uForceP	–	–0.615	–0.581	–0.564	–0.585	–0.617	–0.514
rDispN	–	0.603	0.789	0.810	0.797	0.625	0.799
rForceN	–	0.934	0.877	0.877	0.835	0.763	0.982
uForceN	–	–0.638	–0.631	–0.629	–0.609	–0.608	–0.631
dmgType	–	Energy	Energy	Energy	Energy	Energy	Energy